Experimental study of mirror nuclei ^{10}Be -^{10}C, ^{11}B -^{11}C and ^{9}Be -^{9}B populated via ^{10}B +^{10}B nuclear reactions

D. Jelavić Malenica,[1,*] M. Milin,[2,†] A. Di Pietro,[3] P. Figuera,[3] A. Musumarra,[3] M. G. Pellegriti,[3] V. Scuderi,[3] N. Soić,[1] S. Szilner,[1] D. Torresi,[3] and M. Uroić[1]

[1] *Division of Experimental Physics, Ruđer Bošković Institute, Zagreb, Croatia*
[2] *Physics Department, Faculty of Science, University of Zagreb, Zagreb, Croatia*
[3] *INFN - Laboratori Nazionali del Sud and Sezione di Catania, Catania, Italy*

The symmetric ^{10}B + ^{10}B reaction provides a unique opportunity to populate high-energy, high-spin states in the mirror pairs ^{10}Be –^{10}C, ^{11}B –^{11}C, and ^{9}Be –^{9}B. Excitation spectra for these systems have been measured and mirror analog states identified, enabling a systematic comparison of their level energies. We find that states in compact shell-model configurations (e.g. members of ground-state rotational bands) show very small mirror energy differences (consistent with standard Coulomb displacement energies), whereas spatially extended cluster-like states exhibit significantly reduced energy gaps consistent with the Thomas–Ehrman shift. In the ^{10}Be –^{10}C pair, a previously unreported level at $E_x = 9.24$ MeV in ^{10}C is observed, which we propose as the isospin analog of the 9.56 MeV 2^+ state in ^{10}Be. In the ^{11}B –^{11}C pair, we report a high-lying state at $E_x = 10.69$ MeV in ^{11}C, mirroring the 11.21 MeV level in ^{11}B which was populated via one-nucleon transfer for the first time. Finally, the observed ^{9}Be –^{9}B mirrors show nearly identical excitation spectra; in particular, strongly populated states follow a $J(J+1)$ energy trend, highest of which are consistent with their assignment as the $9/2^-$ members of the ground-state rotational band. These findings highlight the interplay of Coulomb and structural effects in mirror nuclei and extend the known level schemes of the nuclei in question.

INTRODUCTION

Mirror nuclei—pairs of isobars where the number of protons in one nucleus equals the number of neutrons in its counterpart—are powerful probes of nuclear structure and isospin symmetry. In an idealized scenario of exact isospin symmetry, as originally proposed by Heisenberg, protons and neutrons differ only in charge, leading to identical energy spectra in mirror nuclei except for a constant Coulomb displacement. Early nuclear models indeed treated proton and neutron states as two manifestations of a single nucleon, predicting mirror symmetry except for electromagnetic effects. Experimentally observed deviations from exact mirror symmetry, typically of the order of tens to hundreds of keV, are predominantly attributed to the Coulomb interaction between protons, reinforcing the near-perfect charge symmetry of the strong nuclear force [1–5].

However, since the pioneering studies of Ehrman [6] and Thomas [7] in the early 1950s, it has been clear that certain analog states in mirror nuclei exhibit energy differences far exceeding expectations based solely on uniform Coulomb displacement energies (CDE). Ehrman's experimental discovery that the first excited state of ^{13}N lies anomalously lower than its mirror counterpart in ^{13}C was explained theoretically by Thomas using the resonance formalism. He attributed this pronounced deviation, now termed the Thomas–Ehrman shift (TES), to differences in the spatial asymptotic behavior of proton and neutron wavefunctions. Specifically, the weakly bound or unbound proton-rich states possess extended spatial distributions that significantly reduce Coulomb repulsion, thus lowering their excitation energies relative to their neutron-rich analogs.

Importantly, a clear distinction must be made between the overall Coulomb displacement energy—defined as the difference in total binding energies between mirror nuclei—and the Thomas–Ehrman shift, which specifically refers to the excitation energy *differences* of individual analog states due to local structural variations. Unlike the CDE, the TES directly probes the configuration of different nucleon orbitals, especially when extended orbitals such as $s_{1/2}$ states are involved, where spatial differences to e.g. p-orbitals significantly affect the Coulomb interaction and energy.

While initially observed in bound single-particle states [8], the TES has since been generalized theoretically and experimentally to include resonant states [9], cluster and molecular-like configurations [10], as well as highly deformed nuclear states [11–14]. These extensions underscore the sensitivity of the TES to diverse structural features beyond simple single-particle orbital differences, highlighting its utility as a probe for complex nuclear configurations. The Generalized Two-Center Cluster Model (GTCM), for instance, highlights nuclei such as ^{10}Be and ^{10}C—modeled as $\alpha + \alpha + 2n$ and $\alpha + \alpha + 2p$ configurations—as excellent candidates to explore how clustering and spatial extension affect Coulomb shifts and mirror symmetry [15]. Despite these theoretical advancements, experimental studies directly comparing such states across mirror pairs remain incomplete.

This work aims to bridge this gap by studying the excitation spectra of three mirror pairs (^{9}Be –^{9}B, ^{10}Be –^{10}C, and ^{11}B –^{11}C), simultaneously populated in the

symmetric ^{10}B + ^{10}B reaction, which involves transfer reactions such as $\pm 1p \mp 1n$, $\pm 1n$, and $\pm 1p$. While these reactions do not necessarily populate states of the same type, they provide a unique opportunity to compare Coulomb-related energy differences across both compact shell-model states and spatially extended cluster configurations. Additional results from this same experiment, including detailed analysis of ^{12}C and ^{13}C states, can be found in Refs. [16, 17].

Nuclei around $A = 10$ exhibit a rich structural coexistence of shell-model, molecular, and cluster phenomena, including exotic states such as haloes and Borromean configurations [18–21], thus making them ideal test cases for understanding Coulomb displacement and clustering effects. Moreover, this mass region has been successfully addressed by advanced ab initio calculations [22–27], offering valuable benchmarks for nuclear structure models.

At higher excitation energies, dense overlapping resonances complicate state identification, posing particular challenges for tracing rotational bands and accessing high-spin members of deformed cluster structures [28–30]. The experimental conditions employed here uniquely enable the investigation of such complex states in mirror nuclei, providing both new experimental insights and stringent tests for theoretical approaches.

The ^{10}B nucleus, used as both beam and target in this experiment, has properties that make it well suited for structural studies. It is one of only five stable nuclei with odd numbers of both protons and neutrons, and it has the highest ground-state spin ($J^\pi = 3^+$) among light nuclei. Its ground state can be described in the shell model as a stretched configuration of two nucleons in the $p_{3/2}$ subshell coupled to maximum spin.

The low-lying spectrum of ^{10}B is largely reproduced by modern shell-model calculations, though the results depend sensitively on the choice of effective interaction [31]. Early calculations relied on the Cohen-Kurath interaction [32], while more recent work [23, 25] emphasized the need to include three-body forces. Cluster models such as the orthogonality condition model (OCM) [33] and antisymmetrized molecular dynamics (AMD) [34] further suggest that even the ground and low-lying states include non-negligible cluster components, such as (^{6}Li$_{\text{g.s.}}$ + α).

EXPERIMENT

The ^{10}B + ^{10}B experiment was conducted at the INFN-LNS facility in Catania, Italy, utilizing the SMP Tandem accelerator to deliver a highly focused ^{10}B beam (beam diameter 1 mm) at energies of 50.0 and 72.2 MeV. While data were collected at both energies, the results presented in this work are based primarily on the 72.2 MeV measurement, as the 50.0 MeV run had a limited statistics. Targets used were composed of ^{10}B, enriched to 99.8%. The reaction products were detected using four

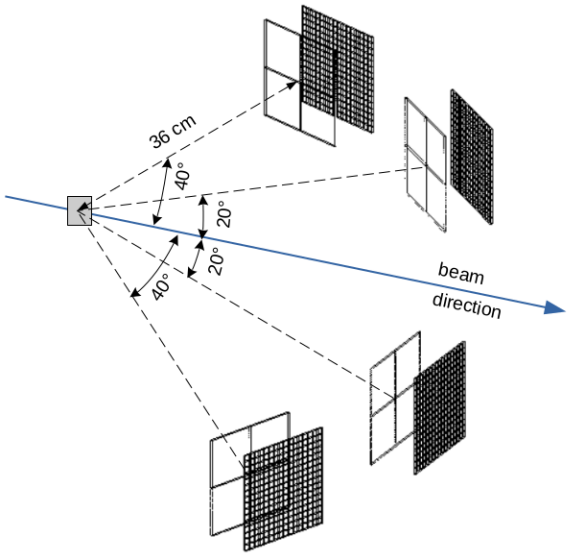

FIG. 1: Schematic view of the detector setup, illustrating the ΔE–E telescopes composed of silicon detectors with four quadrants at the front and double-sided silicon strip detectors (DSSSDs) at the back. Each telescope was positioned 36 cm from the target. The angles shown correspond to one set of azimuthal positions; in total, three azimuthal sets were used during the experiment.

ΔE-E silicon telescopes, each comprising a thin ΔE detector divided into four quadrants, with a thickness of 57-67 μm and a thick double-sided silicon strip detector (DSSSD) with thicknesses of either 500 or 1000 μm. Each DSSSD was segmented into 16 strips on both the front and back faces, allowing for high angular resolution and effective background reduction by requiring the difference between front and back signals to be within a 3% tolerance. A schematic view of the detector setup is illustrated in Fig. 1.

To optimize detection across a variety of reaction exit channels and excitation energies, three distinct detector arrangements were implemented, with polar angles of the detector centers ranging from 20° to 53°. Data were recorded in both single and coincidence modes. The elastic channel and a few nucleon stripping channels were populated with sufficiently high statistics. Notably, the number of detected α-particles significantly exceeded that of other detected nuclei (see Fig. 2). This effect was particularly pronounced in coincident events, with substantial statistics for triple α-particle coincidences recorded. The ΔE-E technique effectively identified isotopes from hydrogen to carbon (Fig. 3).

Monte Carlo simulations were employed to evaluate

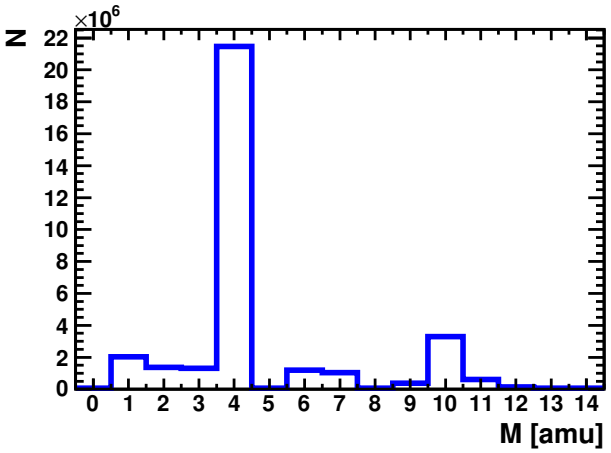

FIG. 2: Mass spectrum of isotopes obtained from the ^{10}B+^{10}B measurement conducted with a 72 MeV beam, using detectors positioned at angles of 40°, 20°, -20°, and -40°. This dataset includes all recorded data, acquired in either single or coincidence mode.

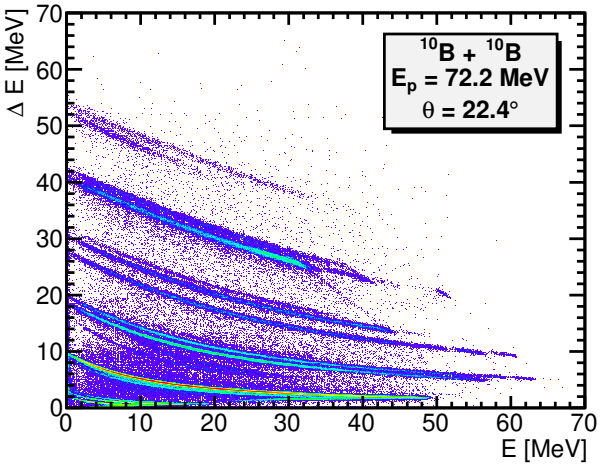

FIG. 3: An example of the ΔE-E spectra for one quadrant of the thin detector and corresponding strips of the DSSSD thick detector in the telescope centered at 22.4°.

detection efficiencies, modeling the two-body ^{10}B +^{10}B reaction under the assumption of isotropic center-of-mass distributions for sequential decay fragments. This simulation framework allowed for reliable estimation of angular acceptance and energy thresholds throughout the experimental setup. Energy and angular resolutions were not included in the simulations. Further details on the experimental setup and isotopic selection can be found in references [16, 17].

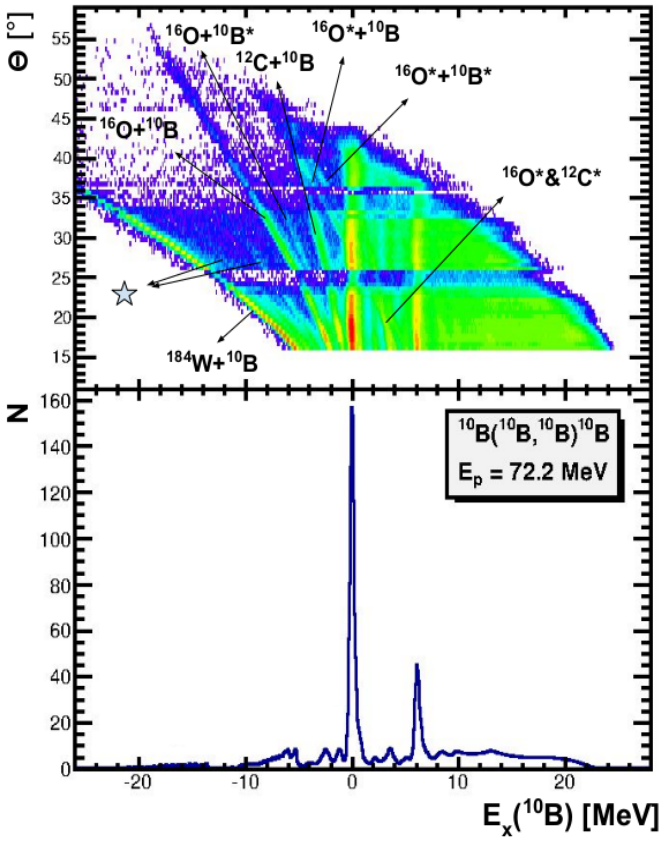

FIG. 4: (*bottom*) Excitation spectrum of ^{10}B from elastic and inelastic scattering of ^{10}B on a ^{10}B target at a beam energy of 72.2 MeV. (*top*) Polar angle dependence of the excitation energy: θ vs. $E_x(^{10}\mathrm{B})$. The contributions of different processes on impurities in the target are marked and explained in detail in the text.

The fitting procedure was done using non-linear least-squares minimization and curve-fitting package for Python lmfit. The background was predefined and fitted using skewed gaussian function, while centroids, widths and amlitudes of the peaks were all free fitting parameters.

RESULTS

Results for ^{10}B and ^{10}C

Although the excitation spectra of ^{10}Be were not directly measured in this experiment, their mirror analogs in ^{10}C can be discussed through the population of corresponding states in ^{10}B, observed in the inelastic channel.

Figure 4 presents the inclusive excitation energy spectrum of ^{10}B, obtained by detecting the recoil ^{10}B nucleus

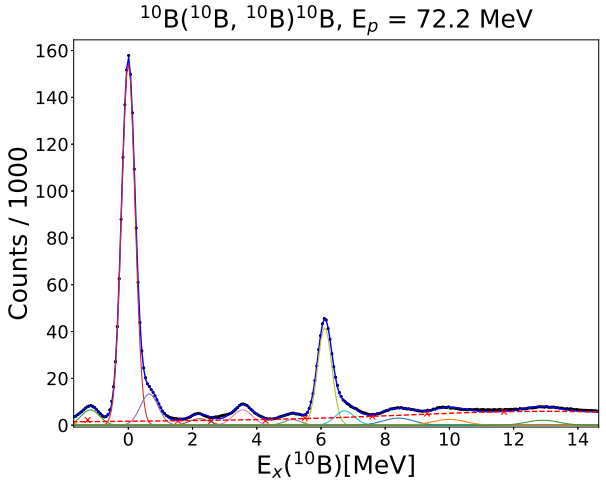

FIG. 5: The inclusive excitation spectrum of ^{10}B obtained by detecting the recoil nucleus ^{10}B, populated through elastic and inelastic channels. Background function is illustrated by the red dotted line. The states are fitted with gaussians on top of the fixed background, resulting in a composed fit indicated in blue.

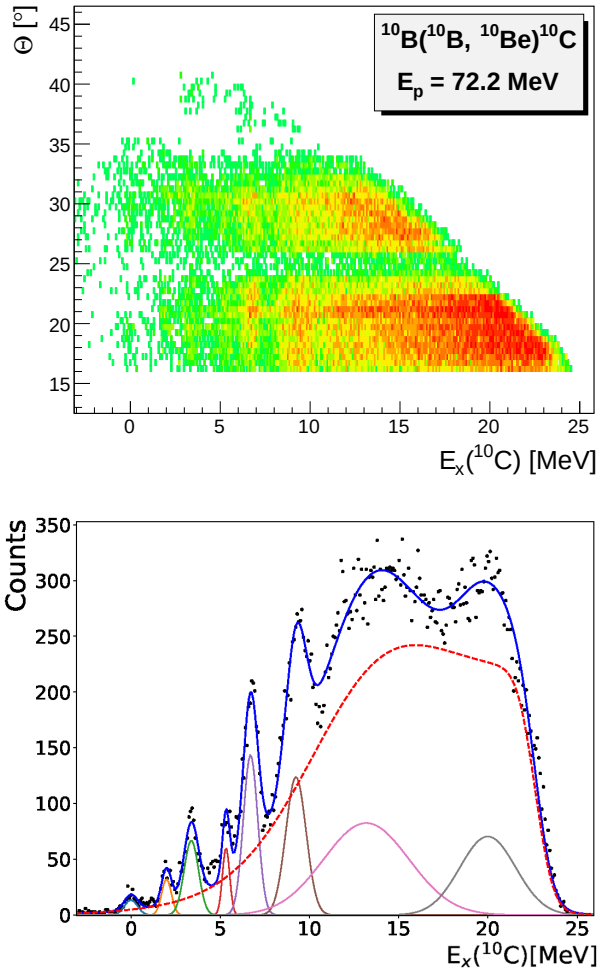

FIG. 6: Inclusive excitation spectrum of ^{10}C obtained by detecting the recoil nucleus ^{10}Be. (*Top*) Polar angle dependence of the excitation energy, shown as a θ vs. $E_x(^{10}\mathrm{C})$ distribution. (*Bottom*) Fitted excitation spectrum of ^{10}C (blue curve), constructed as a superposition of Gaussian peaks (various colors) on top of a fixed background (red). To improve the overall fit quality, two broad Gaussians centered around 13.5 and 20 MeV are included to reproduce the high-energy tail, but are not interpreted as excited states of ^{10}C.

populated via elastic and inelastic scattering channels. The upper part of the figure displays the angular dependence of the excitation energy, aiding in the identification of authentic ^{10}B states.

The boron targets used in the experiment had a thin (4 μg/cm^2) formvar ($C_5H_8O_2$) subtrate, and therefore we see scattering on carbon and oxygen in the target - in Fig. 4 these events are marked accordingly. At ^{12}C we see elastic scattering and inelastic scattering to the first excited state (E_x= 4.44 MeV). At ^{16}O in target we also see elastic and inelastic scattering, but also events corresponding to the inelastic excitation of the ^{10}B projectile to the first excited state (weak line between elastic scattering at ^{16}O and ^{12}C). We also see elastic scattering on ^{184}W and some other lighter metals, present in the target in small amounts due to the manufacturing process - those are marked with a star symbol in Fig. 4. After projection, all the inelastic scattering events contribute to the background visible in the lower part of the figure.

Figure 5 presents the fitted excitation spectrum of ^{10}B, including the background and individual Gaussian components. The background was predefined and fitted using a skewed Gaussian function, while the centroids, widths, and amplitudes of the peaks are all free fitting parameters. The energy resolution in the inclusive spectra is estimated to be 300 keV, as discussed in Ref. [17].

At first glance, strong excitations of the ground state and the state measured at 6.12 MeV are observed, with the latter comprising a combination of three closely spaced levels: 2^+, 4^+, and 3^- at 5.920, 6.025, and 6.127 MeV [35]. This peak is always the strongest one in the inelastic scattering spectra, although the three states are usually inseparable. When resolved [36], it can be seen that the strongest contribution comes from the 4^+ state at 6.025 MeV, which has two valence particles in the $d_{5/2}$ orbital.

By careful background modeling and peak extraction, several additional states were successfully resolved. Among these are important $T = 1$ states, which represent analog states to corresponding levels in ^{10}Be. Given the central focus of this study on mirror nuclei, the clear

identification of these $T = 1$ excitations is crucial for the comparative analysis that follows.

Further analysis of the measured excitation energies, after background subtraction, confirms a series of known ^{10}B states [35], reinforcing the reliability of the extracted spectrum. The state at 0.65 MeV corresponds to the known 1^+ level at 0.718 MeV, while the peaks at 2.21 MeV and 3.56 MeV align with the listed 1^+ and 2^+ states at 2.154 MeV and 3.587 MeV, respectively.

Regarding the 3.56 MeV peak, part of the events contributing to this peak may originate from mutual excitation of both ^{10}B nuclei to the 1.74 MeV $T = 1$ state, corresponding to a double spin-isospin flip reaction: ^{10}B(^{10}B, ^{10}B$^{T=1}$)^{10}B$^{T=1}$ (Q = -3.48 MeV). While a direct estimation of the contribution of this process is challenging, a comparison with the population of the ^{10}C ground state in the analog channel ^{10}B(^{10}B, ^{10}Be$^{T=1}$)^{10}C$^{T=1}$ (Fig. 6) suggests that the spin-isospin flip process is present at a low but non-negligible level.

At higher excitation energies, multiple closely spaced states appear, making it challenging to distinguish individual contributions within our energy resolution. The 5.10 MeV peak likely corresponds to a combination of the 2^- and 1^+ states at 5.11 and 5.180 MeV (the 2^+ state at 5.164 MeV has isospin $T = 1$). Another interesting peak is the shoulder of the pronounced 6.12 MeV state, centered at 6.74 MeV with a width of 300 keV (the broadening due to the strong excitation of the nearby 6.12 MeV state must be taken into account). The closest known states are 6.560 MeV for which the high spin, 4^-, is suggested [37] and rarely observed state at 6.873 MeV, discussed in terms of isospin mixing [38].

Peaks at even higher excitation energies suggest contributions from mutual excitation. The 8.41 MeV peak may correspond to a single-particle excitation, with the closest candidates being the 3^+ state at 8.68 MeV. However, it could also result from mutual excitation, involving the 2^+ state at 3.587 MeV coupled with one of the closely spaced states near 5.1 MeV, or the 1^+ state at 2.154 MeV combined with one of the states near 6.0 MeV.

Similarly, the very wide peak at 9.99 MeV could correspond to a single excitation to the $T = 0$ state at 9.58 MeV or the nearby 10.84 MeV state with undefined isospin [39]. Alternatively, it may originate from mutual excitation involving the 3.568 MeV and 6.0 MeV states.

To explore the isotopic shift of cluster levels in mirror nuclei for the $A = 10$ ($T = 1$) system, a detailed understanding of the ^{10}C level scheme is essential. Despite the experimental challenges associated with producing and detecting ^{10}C, the present study successfully provides a well-resolved ^{10}C excitation spectrum using a relatively simple reaction mechanism.

Figure 6 presents the inclusive excitation spectrum of ^{10}C, reconstructed from detected ^{10}Be nuclei (selected via narrow graphical cut to separate from much stronger ^{9}Be - see Fig. 3). The ability to obtain such a high-quality ^{10}C spectrum is particularly significant, as previous studies have been hindered by low statistics and substantial background contamination. Here, the background events (bottom part of Fig. 6) originate from several sources, including contributions from three-body channels, the inability to separate ^{10}Be from ^{9}Be. The Q-values for the (^{10}B,^{10}Be) reactions on the ^{12}C and ^{16}O impurities in the target are equal to -17.90 and -15.97 MeV, respectively, so there is no contribution of these reactions in the energy range studied here.

The measured excitation energies of ^{10}C in this experiment are 0.0, 3.38, 5.32, 6.70, and 9.24 MeV. A structure observed around 2.1 MeV is not attributed to a genuine ^{10}C state, but has been thoroughly investigated and confirmed to originate from ^{9}Be events leaking through the ^{10}Be selection cut. The ground-state transition corresponds to the previously mentioned double spin-isospin flip transition. The strong peak observed at 3.38 MeV corresponds to the first excited 2^+ state in ^{10}C (3.356 MeV), with an excitation energy nearly identical to that of its analog in ^{10}Be (3.368 MeV). Due to limited experimental energy resolution (approximately 300 keV), these states, separated by only 12 keV, cannot be distinguished. Nevertheless, the presence of either one or the other excitation within this reaction channel is fully consistent with expectations based on their established level schemes [35].

At higher excitation energies, closely spaced states emerge, challenging unambiguous identification. These peaks may include contributions from mutual excitations of both reaction partners or minor contamination from the ^{9}Be isotope, although isotope separation in this experiment is effectively controlled. Specifically, the peaks at 5.32 MeV and 6.70 MeV lie in regions populated by several closely spaced states previously reported in the literature [43–45], precluding definitive identification. For the 5.32 MeV state, three nearby states are listed: a 2^+ state at 5.22 MeV, a 0^+ state at 5.29 MeV, and a 2^- state at 5.38 MeV. Similarly, the 6.70 MeV peak lies near a 3^- state at 6.55 MeV and a 2^+ state at 6.57 MeV. Due to the experimental resolution and level density in this energy region, it is likely that each observed peak represents a superposition of two or more unresolved transitions.

The peak observed at the highest excitation energy of 9.24 MeV, with a measured width of 570 keV, does not match any previously reported level in the established ^{10}C excitation spectrum. Its significant strength and energy position make it unlikely to originate solely from mutual excitations or background contributions. The only combination of mutual excitations that gives energies near 9.24 MeV is that in which ^{10}Be is populated into the doublet at 5.96 MeV and ^{10}C into the first excited state at 3.35 MeV. But the doublet and other states around 6 MeV in ^{10}Be are not visible at all in Fig. 6, which is consistent with their known well-pronounced

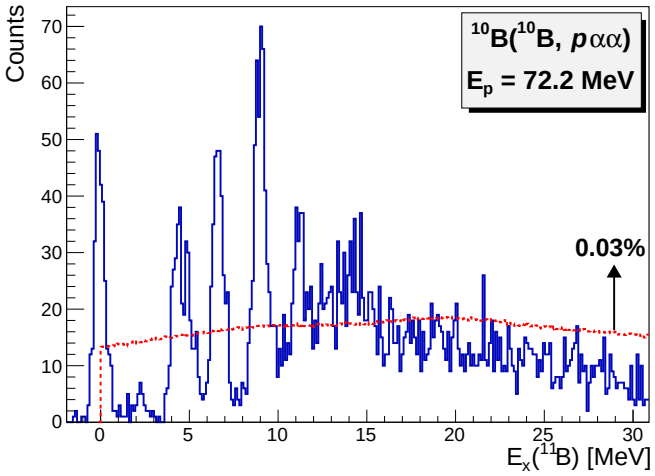

FIG. 7: Excitation spectrum of ^{11}B obtained by triple coincidence detection of two α-s and proton. All three particles are detected in the same detector, at 20° or 30°. The (red) dotted line shows the corresponding Monte Carlo efficiency curve. The absolute value of efficiency is given for a single point of the curve, so that it can be inferred for the rest of it.

cluster/molecular structure (see e.g. Ref. [19]) and the fact that they are never significantly populated in the inelastic scattering because their structure is different from the g.s. structure. We don't therefore expect any significant contribution of mutual excitation to the 9.24 MeV peak. Instead, its clear and isolated appearance strongly suggests the presence of a new resonance, which will be further discussed in the context of mirror symmetry and potential analog assignments. Of course, the possibility that the observed peak corresponds to two states at ^{10}C cannot be ruled out, but the data do not offer solid evidence for such a claim.

The results presented here highlight the power of the ^{10}B +^{10}B reaction in accessing ^{10}C states, providing valuable data in a region where experimental information has been historically scarce.

Results for ^{11}B and ^{11}C

The advantage of the highly segmented strip detector setup for multi-particle coincidence studies is well demonstrated in Fig. 7, which presents an excitation spectrum of ^{11}B reconstructed from triple coincidence events α+α+p. The reconstruction is based on the following constraints:

(i) The two detected α-particles have a relative energy corresponding to the ground state of ^{8}Be.

(ii) The reconstructed ^{8}Be and proton exhibit relative motion corresponding to the ground state of ^{9}B.

No other ^{9}B state is clearly identified in the data, as shown in Fig. 8. This selection uniquely isolates ^{11}B states populated via the reaction ^{10}B(^{10}B,^{9}B$_{g.s.}$)^{11}B, a process that has never been observed before due to the fact that ^{9}B is particle-unbound. The ability to reconstruct such a reaction represents a significant advancement, offering an unprecedented opportunity to probe the ^{11}B excitation spectrum under these specific conditions.

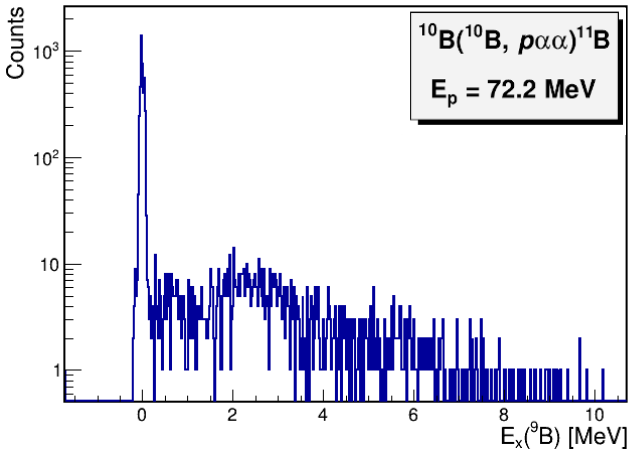

FIG. 8: Excitation spectrum of ^{9}B obtained by detecting 2 α-particles and a proton in coincidence, inside the same detector, with additional cut that two α-s are coming from the ^{8}Be ground state. Results for both front detectors at 20° and 30° are combined.

All three decay products of ^{9}B—two α-particles and a proton—are detected within the same telescope at forward angles (20° or 30°). This is a direct consequence of the fact that the ^{9}B decay products emerge with very low relative energy, essentially preserving the original motion of the parent ^{9}B nucleus.

The red/dotted line in Fig. 7 represents the Monte Carlo simulated efficiency for triple-coincidence detection. It is obtained from a simulation modeling the ^{10}B + ^{10}B reaction as a two-body process with an isotropic distribution in the center-of-mass frame, followed by sequential decay into fragments, also assumed to be isotropic in the center-of-mass frame. The simulation incorporates both angular constraints to replicate the acceptance of the detectors and energy thresholds to account for detection limitations.

For this specific spectrum, the energy resolution is consistent with other spectra obtained from coincidence measurements (≈200 keV) [17]. The states populated in Fig. 7 include the ground state, as well as excitations at 2.27, 4.34, 4.89, 6.64, 9.02 and 11.21 MeV. These correspond to the tabulated levels [46]: the $3/2^-$ ground state, the $1/2^-$ state at 2.125 MeV, the $5/2^-$ state at 4.445

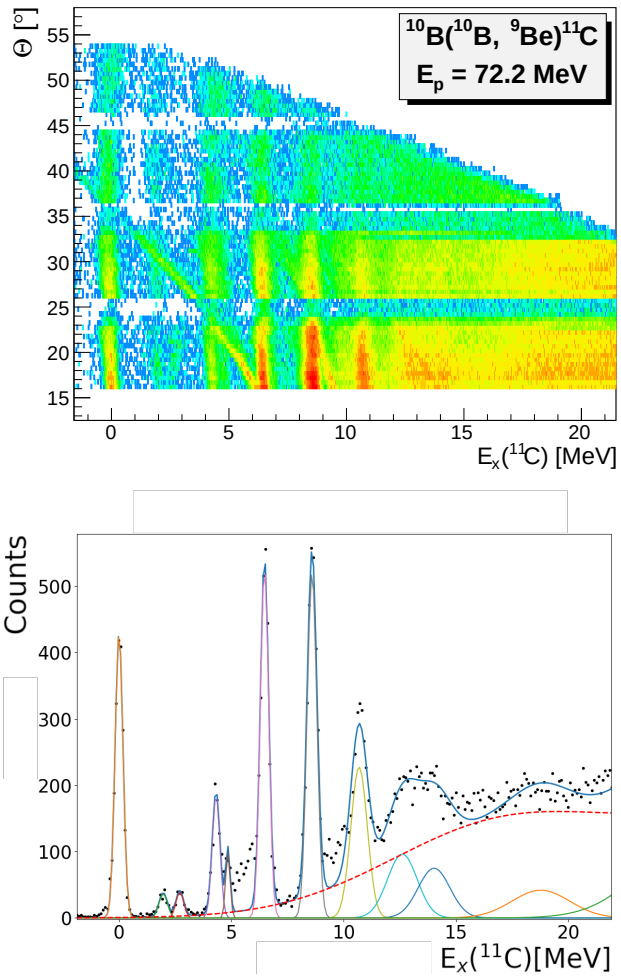

FIG. 9: Inclusive excitation spectrum of ^{11}C obtained by detecting the recoil nucleus ^{9}Be. (*Top*) Polar angle dependence of the excitation energy, shown as a θ vs. $E_x(^{11}\mathrm{C})$ distribution. (*Bottom*) Fitted excitation spectrum of ^{11}C (blue curve), constructed as a superposition of Gaussian peaks (various colors) on top of a fixed background (red). In order to improve the overall fit, two broad Gaussians in the high-energy region (around 13, and 19.5 MeV) are added to the background, but are not considered to be the excited states of ^{11}C.

MeV, the $3/2^-$ at 5.020 MeV, the $7/2^-$ state at 6.742 MeV, unresolved $5/2^-$ and $7/2^+$ states near 9 MeV, and probably the $9/2^+$ state at 11.272 MeV. Notably, the 11.21 MeV state is of particular interest, as this might be the first evidence of its excitation via single-nucleon transfer reaction channel. It is also possible that multiple ^{10}B states contribute to this peak.

Inclusive excitation spectrum for ^{11}C populated through reaction ^{10}B(^{10}B,^{9}Be)^{11}C at beam energy 72.2 MeV is shown in Fig. 9. The ^{9}Be nucleus has no particle stable excited states – mutual excitations are therefore not possible in this channel. Four strong peaks are observed at 0.0, 4.32, 6.48, and 8.59 MeV in ^{11}C (the last peak likely comprises two unresolved states), and all are in good agreement with [46]. Besides these, there are also two less pronounced states at 1.97 and 4.84 MeV, also in agreement with listed values [46], and a high energy state at 10.69 MeV, which is the most interesting state here.

At higher energies, peaks at 12.62 MeV and 14.03 MeV can be seen in Fig. 9, although they could be better resolved if the angles before projection were limited to values between 25 and 45 degrees - these peaks probably correspond to the known ^{11}C states at 12.65 and 14.07 MeV.

Other structures are also visible, including a peak near 3 MeV. However, based on angular distribution analysis (see the upper panel of Fig. 9), these features do not originate from the ^{11}C channel, but are instead associated with reactions on target impurities or backing material, rather than the ^{10}B itself. Although Gaussian components were included in the overall composite fit to account for these contributions and improve the fit quality, they are excluded from the discussion of ^{11}C states. Similarly, two additional broad Gaussians used to model the background at higher excitation energies are also not considered part of the ^{11}C level structure.

Results for ^{9}Be and ^{9}B

The inclusive spectra for nuclei ^{9}Be and ^{9}B, derived from the ^{11}C and ^{11}B particles detected by any of the four telescopes individually, are shown in Fig. 10 and 11.

The excitation spectrum of ^{9}Be in Fig. 10 shows clear peaks corresponding to the ground state and excited states at 2.48, 4.45, 6.89 and 11.46 MeV. Four of the observed states correspond to well-established ^{9}Be levels: the $3/2^-$ ground state, the $5/2^-$ state at 2.429 MeV, the $3/2^+$ state at 4.704 MeV, and the $9/2^-$ state at 11.283 MeV. The latter two, however, still carry some ambiguity in their spin-parity assignments. The peak observed at 6.89 MeV likely results from an unresolved blend of the $7/2^-$ state at 6.38 MeV and the $9/2^+$ state at 6.76 MeV. It can also have contributions from mutual excitations. The 2.48 MeV state, although intrinsically narrow, appears broadened in the current measurement due to background contamination from other reaction channels. Additionally, the nearby 4.45 MeV state is affected by asymmetric background contributions, which may cause its shift toward lower excitation energy.

As the excitation energy increases, the spectrum becomes increasingly affected by a steeply rising background, due to the onset of additional reaction channels and possible contributions from target impurities. In the upper part of Fig. 10, a very broad bump is observed

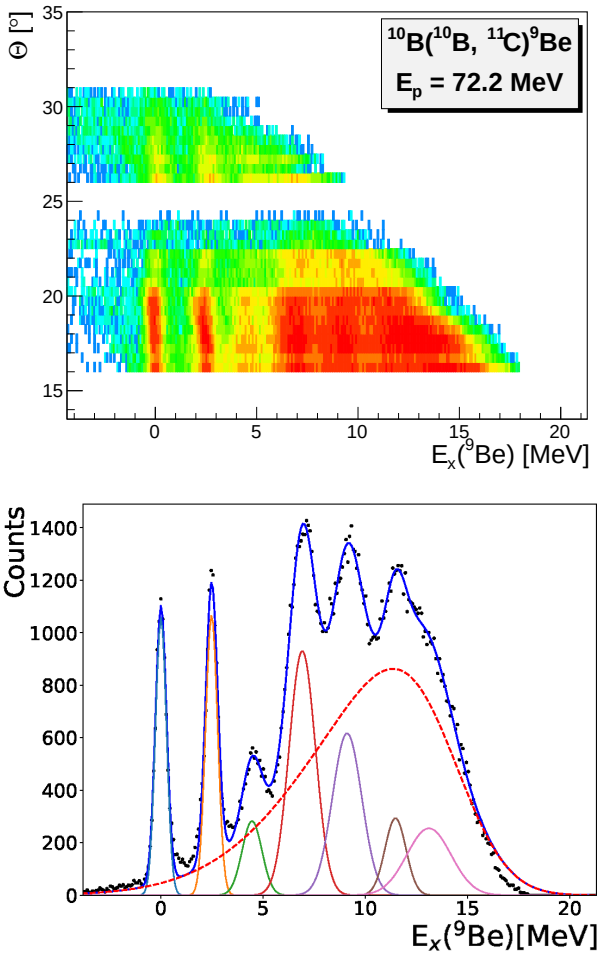

FIG. 10: Inclusive spectrum of ^{9}Be obtained by detecting the recoil nucleus ^{11}C. (*Top*) Polar angle dependence of the excitation energy, shown as a θ vs. E_x(^{9}Be) distribution. (*Bottom*) Fitted excitation spectrum of ^{9}Be (blue curve), constructed as a superposition of Gaussian peaks (various colors) on top of a fixed background (red). A broad Gaussian around 13.5 MeV is added to the background but not interpreted as an excited state of ^{9}Be.

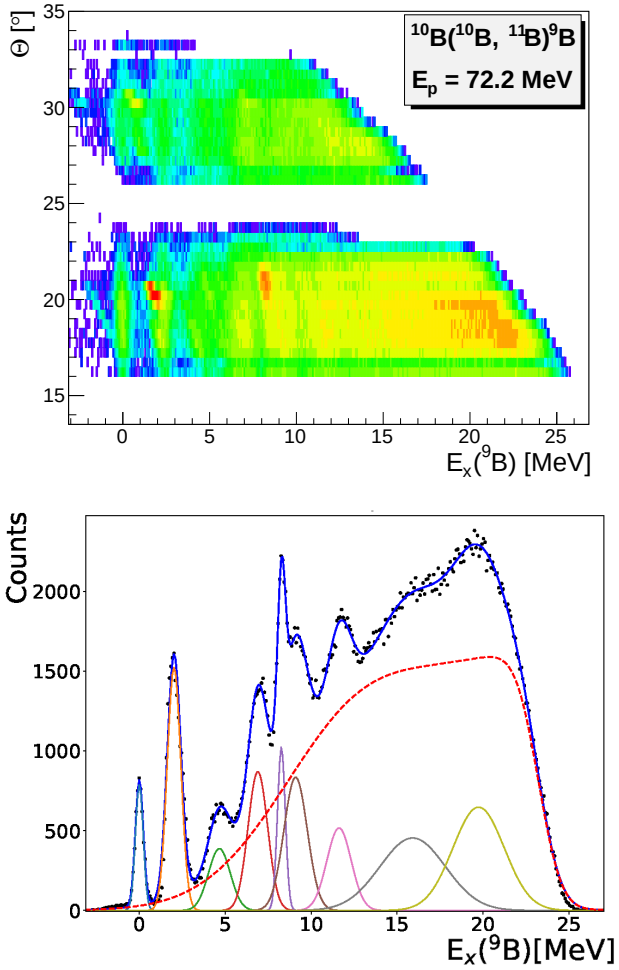

FIG. 11: Inclusive spectrum of ^{9}B obtained by detecting the recoil nucleus ^{11}B. (*Top*) Polar angle dependence of the excitation energy, shown as a θ vs. E_x(^{9}B) distribution. (*Bottom*) Fitted excitation spectrum of ^{9}B (blue curve), constructed as a superposition of Gaussian peaks (various colors) on top of a fixed background (red). Broad Gaussians around 15.5 and 19.2 MeV are included in the background but are not considered excited states of ^{9}B.

around 10 MeV. Its diffuse shape and lack of structure suggest that it does not originate from ^{9}Be, but rather from mutual excitations or background processes, likely involving ^{11}C. In contrast, the 11.46 MeV peak appears as a well-defined structure with an asymmetric background on the low-energy side. Its clear separation from the surrounding continuum and consistent shape support its identification as a genuine state populated through the primary reaction channel, rather than as a result of mutual excitation or impurity contributions.

The inclusive excitation spectrum of ^{9}B, shown in Fig. 11, displays well-defined peaks at 0.0, 2.32, 4.58, 6.85, and 11.59 MeV. The ground state is clearly identified with minimal background contamination. The strongly populated state at 6.85 MeV is a mixture of the $7/2^{-}$ state in ^{9}B at 6.97 MeV and the ^{11}B excitation at 6.74 MeV [35], while the broad structure near 8–9 MeV surely originates from mutual excitations.

The peak at 2.32 MeV is primarily associated with the $5/2^{-}$ state in ^{9}B [35], but its centroid appears shifted due to contributions from the 2.12 MeV state in ^{11}B. Additional contamination from events unrelated to the ^{9}B states, which can be clearly separated in the detector at 30°, further broadens this peak (the upper part of

Fig. 11). Therefore, a separate fit was performed for this detector to mitigate these effects.

The structure at 4.58 MeV is more complex, likely incorporating contributions from reactions on oxygen impurities, the 4.45 MeV state in ^{11}B, and possible mutual excitations involving ^{9}B at 2.36 MeV and ^{11}B at 2.12 MeV [35]. The peak at 6.85 MeV is attributed primarily to the well-established $7/2^-$ state in ^{9}B (which has $\Gamma = 2000$ keV), with only minor influence expected from nearby ^{11}B states. A weaker feature just above 8 MeV appears to stem from ^{10}B contamination rather than an intrinsic ^{9}B excitation.

Finally, the peak at 11.59 MeV is primarily attributed to a ^{9}B state, though contributions from mutual excitations cannot be excluded. Background effects and the proximity to the detection threshold also influence this region.

DISCUSSION

Mirror states in ^{10}Be – ^{10}C pair

Among the three mirror pairs addressed in this work, the ^{10}Be–^{10}C system presents the greatest challenge. The ^{10}Be excitation spectrum is not directly measured in this experiment; instead, conclusions are inferred through the states known to be analog states of those populated in ^{10}B via inelastic scattering. It is worth noting that ^{10}C is a nucleus that is experimentally challenging to produce; nevertheless, a remarkably clean excitation spectrum has been obtained in this case (Fig. 6). For completeness, all three mirror pairs are included in the discussion to provide a broader structural overview.

A comprehensive list of analog states in $A = 10$ nuclei is provided in Table I. The population of the ^{10}C ground state in the ^{10}B(^{10}B, ^{10}Be$^{T=1}$)^{10}C$^{T=1}$ channel (Fig. 6) supports the presence of the spin-isospin flip process. In this reaction, the lowest $T = 1$ state in ^{10}B is populated, which is considered the analog to the ground states of ^{10}Be and ^{10}C in the context of mirror symmetry. By comparing the yields of the ^{10}B and ^{10}C ground states, we estimate that approximately 1% of the events in the 3.56 MeV ^{10}C peak arise from mutual excitation of the $T = 1$ state at 1.74 MeV in both ^{10}B nuclei (i.e., a $1.74 \otimes 1.74$ configuration). This estimated contribution is marked with an asterisk in Table I.

Meaningful comparisons of excitation energies in mirror nuclei rely on referencing energy differences relative to a compact baseline—typically the ground state. In this framework, standard Coulomb displacement effects account for the general offset between mirror analogs. However, when this shift is significantly reduced, it may indicate the presence of the Thomas–Ehrman shift (TES), arising from differences in the spatial extent of the wavefunction in the proton-rich partner.

A clear example of compact, shell-model-like structure is provided by the first 2^+ states in ^{10}B, ^{10}Be, and ^{10}C. The state in ^{10}B is observed at 5.10 MeV (Fig. 5), corresponding to an excitation of 3.36 MeV above its lowest $T = 1$ state. Its analogs appear at 3.38 MeV in ^{10}C (Fig. 6) and 3.368 MeV in ^{10}Be, with nearly identical energies. The small mirror splitting confirms their compact nature and highlights the absence of any significant TES effect.

A contrasting case is seen in cluster-type configurations. The second 0^+ state in ^{10}C, observed at 5.32 MeV, lies significantly below its mirror state in ^{10}Be at 6.179 MeV. Several theoretical models, including the antisymmetrized molecular dynamics combined with the Hartree–Fock method [40], the molecular orbit model [41], and the microscopic four-cluster model [42], suggest that the second 0^+ state in ^{10}Be corresponds to a spatially extended structure with a large separation between the two α particles. The observed 860 keV Coulomb shift between ^{10}Be and ^{10}C in the present measurement is in excellent agreement with predictions from Generalized Two-Center Cluster Model (GTCM) calculations by M. Ito [15], which estimate a shift of approximately 1 MeV. The suppressed Coulomb repulsion associated with the extended geometry in ^{10}C leads to a lower excitation energy compared to its mirror in ^{10}Be. This example illustrates the TES as a structural probe, sensitive to differences in spatial configuration between mirror nuclei. Given the theoretical expectations and the observed energy shift, the 5.32 MeV peak in ^{10}C remains a promising candidate for the mirror of the ^{10}Be 0^+_2 state.

Another example of close spacing between excitations of relevant mirror states occurs in the region around 6.7 MeV in ^{10}C. According to Refs. [44, 47], two $T = 1$ levels are reported in ^{10}C at 6.55 MeV (3^-) and 6.57 MeV (2^+). In the present measurement, we observe a peak at 6.70 MeV, which likely represents a superposition of these two unresolved states. Their analogs in ^{10}Be are the 3^- state at 7.371 MeV and the 2^+ state at 7.542 MeV, both of which also have $T = 1$.

A similar situation is observed in ^{10}B, where a peak at 8.41 MeV appears in the inclusive excitation spectrum (Fig.5). This energy matches the expected mirror counterparts of ^{10}Be and ^{10}C states discussed above. The $T = 1$ state at 8.9 MeV in ^{10}B, assigned as the analog of the 7.54 MeV (2^+) level in ^{10}Be and observed in the ^{1}H(^{9}Be, α)^{6}Li* reaction [47], is also seen in the present data. Given the small energy separation between the 3^- and 2^+ states in all three nuclei, it is not possible to distinguish between them. Both are $T = 1$ states accessible through the same reaction mechanism, and are therefore expected to contribute to the observed peaks.

Although there is selective excitation of states in the spectra due to the reaction mechanism being dominantly nucleon transfer, the selectivity is less pronounced than in sequential decay reactions. Under such conditions, states

TABLE I: Analog states in ^{10}Be, ^{10}B and ^{10}C. For the ^{10}B and ^{10}C nuclei, two columns are provided: the excitation energy measured in this study and the values listed in [45]. For the ^{10}B column, numbers in brackets represent the excitation energy of the states relative to the lowest T=1 state at 1.74 MeV.

J^π	$E_x(^{10}\text{Be})$ [MeV][45]	$E_x(^{10}\text{B})$ [MeV]	$E_x(^{10}\text{B})$ [MeV][45]	$E_x(^{10}\text{C})$ [MeV]	$E_x(^{10}\text{C})$ [MeV][45]
0^+	g.s.	1.78*	1.740 (0.00)	0.00	g.s.
2^+	3.368	5.10	5.164 (3.42)	3.38	3.354
0^+	6.179		7.560 (5.82)	5.32	5.29
3^-, 2^+	7.371, 7.542	8.41	8.889 (7.15), 8.894(7.20)	6.70	6.55, 6.57
2^+	9.56	9.99	10.84 (9.10)	9.24	

of different spin and parity may be populated with comparable strength. The peak at 6.70 MeV in ^{10}C—and its analogs in ^{10}Be and ^{10}B—is thus interpreted as a combined contribution from the two closely spaced $T = 1$ levels (3^- and 2^+), rather than a single, isolated excitation.

The most significant result of this study is the observation of a previously unreported state in ^{10}C at $E_x =$ 9.24 MeV. This peak has no clear counterpart in the existing ^{10}C level compilations [35] or recent experimental studies [30, 44], yet its energy aligns closely with the well-established 2^+ state in ^{10}Be at 9.56 MeV, which has been observed in numerous measurements [43, 48, 49] and is described successfully within the shell-model framework [24]. It was found to be the only ^{10}Be state that shows comparable decay strengths through both the ^{9}Be+n and the ^{6}He+α channels [28, 29, 50]. This close energy correspondence strongly suggests that the 9.24 MeV state in ^{10}C is its isospin analog. The absence of any prominent peak near 6 MeV in the present spectrum further supports this interpretation, as it implies that the observed structure does not result from mutual excitation processes.

A state in ^{10}C near 9 MeV was previously reported in a reanalysis of the ^{10}B(p,n)^{10}C reaction [51]. More recently, a level at 9.647 MeV was observed in [30] and interpreted as a member of a highly deformed rotational band built on the second 0^+ state, associated with a pronounced molecular structure involving valence protons. In contrast, the 9.24 MeV state observed in the present experiment exhibits a significantly smaller Coulomb displacement relative to the mirror state in ^{10}Be—traced via the analog ^{10}B level at 9.99 MeV—suggesting a more compact, shell-model-like structure. This distinction indicates that the state reported here is different from the 9.647 MeV molecular candidate [30] and likely represents a new resonance in ^{10}C.

Mirror states in ^{11}B - ^{11}C pair

The ^{11}B–^{11}C mirror system is among the best studied light nuclear pairs, yet some key structural ambiguities remain. Despite decades of investigation [52–55], the isospin assignment of several higher-lying states remains uncertain, with conflicting reports favoring either T=1/2 or T=3/2. Such discrepancies are often attributed to isospin mixing—an effect that plays a central role in understanding nuclear structure [56].

Table II summarizes the analog states populated in this work. The excitation energies show good agreement with the latest compilation of ^{11}B and ^{11}C levels [46]. Small deviations (up to 200 keV) in the measured ^{11}B levels from tabulated values are attributed to uncertainties in the reconstruction process but do not affect the overall pattern of mirror symmetry observed.

Four prominent ^{11}C states are observed at 0.0, 4.32, 6.48, and 8.59 MeV, mirrored by states in ^{11}B at 0.0, 4.34, 6.64, and 9.02 MeV, respectively. Additionally, weaker peaks in ^{11}C at 1.97 and 4.84 MeV correspond to ^{11}B states at 2.27 and 4.89 MeV. All six pairs agree with reference values within 100–200 keV [46]. These negative-parity, low-lying levels are typical of shell-model configurations, consistent with the more compact structure of the ^{11}B and ^{11}C ground states. In contrast, positive-parity states in these nuclei tend to exhibit clustering and large deformations, forming two rotational bands as proposed in [56].

The observed strong population of these states aligns with earlier transfer reaction studies such as ^{10}B(^{3}He,d)^{11}C [58, 59] and ^{10}B(d,n)^{11}C [60, 61], confirming the selectivity of the one-nucleon transfer mechanism. In the mirror symmetry framework, this selectivity favors spherical shell-model states with similar $p_{3/2}$ proton/neutron configurations.

In compact configurations, the excitation energy differences ΔE between analog states primarily reflect standard Coulomb displacement effects. For states belonging to the same rotational band as the ground state, ΔE is typically small (around 0.1 MeV), as predicted by microscopic three-cluster models such as [14]. Our observations are consistent with such expectations, reinforcing the interpretation of these states as compact and symmetric, with the observed ΔE values reflecting standard Coulomb displacement energies rather than exhibiting features characteristic of the Thomas–Ehrman shift.

The structure near 8.6–9.0 MeV in both nuclei appears

TABLE II: Analog states in ^{11}B and ^{11}C. For each nuclei two columns are provided: the excitation energy measured in the present experiment and the values listed in [46].

J^π	$E_x(^{11}\mathrm{B})$ [MeV]	$E_x(^{11}\mathrm{B})$ [MeV] [46]	$E_x(^{11}\mathrm{C})$ [MeV]	$E_x(^{11}\mathrm{C})$ [MeV][46]
$3/2^-$	0.00	g.s.	0.00	g.s.
$1/2^-$	2.27	2.125	1.97	2.0
$5/2^-$	4.34	4.445	4.32	4.319
$3/2^-$	4.89	5.020	4.84	4.804
$7/2^-$	6.64	6.742	6.48	6.478
$5/2^-$, $7/2^+$	9.02	8.92, 9.18	8.59	8.420, 8.654
$9/2^+$	11.21	11.272	10.69	10.679

as unresolved peaks, most likely a mixture of $5/2^-$ and $7/2^+$ states. These are tabulated at 8.92 and 9.18 MeV in ^{11}B and at 8.42 and 8.65 MeV in ^{11}C [46]. Their proximity and overlapping widths explain the inability to distinguish between them, but their mirrored population suggests a similar underlying configuration.

In contrast, the 8.1 MeV state in ^{11}C, often associated with exotic cluster configurations, is not observed in this reaction. This is consistent with the expected selectivity of single-nucleon transfer, which is not efficient at populating such states. Interestingly, the same state is populated in the α + ^{7}Be exit channel of the same experiment [62], where additional data selection is achieved through coincidence analysis, further supporting its interpretation as a molecular configuration.

At higher excitation energies, we observe a high-spin mirror pair at 10.69 MeV in ^{11}C and 11.21 MeV in ^{11}B. These correspond to the $9/2^+$ states listed at 10.679 MeV and 11.272 MeV in [46], and this is the first time the latter has been observed in a one-nucleon transfer reaction. They have previously been reported in cluster-favoring reactions such as: ^{7}Li(^{9}Be,^{11}B$^*\rightarrow\alpha+^7$Li)^{5}He and ^{16}O(^{9}Be,^{11}C$^*\rightarrow\alpha+^7$Be)^{14}C, as well as in Refs. [52–54]. The clear observation of this mirror pair in our data demonstrates the sensitivity of our setup to high-spin states and the usefulness of the ^{10}B +^{10}B reaction in accessing them.

These results also resonate with theoretical predictions. Antisymmetrized Molecular Dynamics (AMD) calculations predict the coexistence of Hoyle-like and molecular states in ^{11}B and ^{11}C, emphasizing the need for experimental evidence to distinguish between localized three-body clusters and delocalized molecular configurations [57].

In summary, the ^{11}B–^{11}C mirror pair displays a high degree of spectral symmetry. Analog states are systematically populated and matched across the two nuclei, including high-spin excitations previously unreported in single-nucleon transfer reactions. The present data provide new benchmarks for both theoretical and experimental studies of mirror symmetry in the $A = 11$ mass region.

Mirror states in ^{9}Be - ^{9}B pair

The analog excitation energies for ^{9}Be and ^{9}B are listed in Table III. Despite a somewhat more complicated experimental background for ^{9}B — mainly due to overlapping contributions from elastic scattering channels and imperfect isotope separation — the analog states in these two nuclei show remarkable similarity. The measured excitation energies align closely with previously tabulated levels [35], reflecting consistent mirror symmetry across this nuclear pair.

The strongest population occurs in states belonging to the well-established ground-state rotational bands ($3/2^-$, $5/2^-$ and $7/2^-$ band members). In the present measurement, the $5/2^-$ state in ^{9}B appears broadened due to background contributions not associated with the primary reaction channel (see Fig. 11). To account for this, an independent fit was performed using data from the detector at 30°, as indicated by an asterisk in Table III.

Outside these rotational bands, only the positive-parity $3/2^+$ states at 4.45 MeV in ^{9}Be and at 4.58 MeV in ^{9}B are observed. Historically, these unnatural-parity states posed theoretical challenges due to their excitation energies being significantly lower than shell-model predictions, likely indicating a nucleon excitation into a higher oscillator shell [63]. In ^{9}Be, the spin-parity assignment for the corresponding state at 4.704 MeV remains uncertain. Proposed assignments include $3/2^-$ [35, 64, 65], $5/2^+$ or $1/2^-$ [66–69], with recent β-decay studies of polarized ^{9}Li favoring a $1/2^-$ assignment [70]. Its mirror counterpart in ^{9}B is observed here at 4.58 MeV and exhibits a width $\approx$ 580 keV, consistent with the previously reported state at 4.3 MeV [71].

Notably absent in both nuclei are the first excited $1/2^+$ cluster states, well-known for their pronounced molecular structures. These levels, predicted to be broad (with widths $\sim$1.5 MeV in ^{9}B [72]), are rarely populated by one-nucleon transfer reactions due to their distinctively different configurations compared to the compact ground-state band.

At higher excitation energies, strong mirror excitations appear at 11.46 MeV in ^{9}Be and 11.59 MeV in ^{9}B. Both states also have comparable widths (around 600 keV),

TABLE III: Analog states in ^{9}Be and ^{9}B. For each nuclei two columns are provided: the excitation energy measured in the present experiment and the values listed in [35].

J^{π}	E_x (^{9}Be) [MeV]	E_x(^{9}Be) [MeV][35]	E_x (^{9}B) [MeV]	E_x(^{9}B) [MeV][35]
$3/2^{-}$	0.00	g.s.	0.00	g.s.
$5/2^{-}$	2.48	2.429	2.32*	2.361
$(3/2)^{+}$	4.45	4.704	4.58	4.3
$7/2^{-}$, $9/2^{+}$	6.89	6.38, 6.76	6.85	6.97
$(9/2^{-})$	11.46	11.283	11.59	11.65

suggesting a common structural origin. As illustrated in Fig. 12, these states follow the characteristic $J(J+1)$ energy trend, strongly supporting their tentative assignment as $9/2^{-}$ rotational band members. The small excitation energy difference of approximately 130 keV between (comparable to the difference among other mirror pairs in the bands) is consistent with the Coulomb displacement expected for compact, rotationally aligned configurations. Unlike the Thomas–Ehrman shift, which would require significant differences in proton and neutron wavefunction distributions, the observed minimal energy difference strongly reinforces the rotational-band interpretation. The bands should thus have rather compact ^{5}He+^{4}He or ^{5}Li+^{4}He structure, similar to the rather compact structure of the ^{10}Be ground state.

Theoretical descriptions of these higher-spin band members remain challenging. State-of-the-art calculations generally predict the $7/2^{-}$ and $9/2^{-}$ states at significantly lower excitation energies than experimentally observed [73].

In summary, the excitation spectra of ^{9}Be and ^{9}B demonstrate pronounced mirror symmetry, especially for the low-lying rotational states and the high-spin candidates around 11.5 MeV. These results provide important constraints for theoretical models aimed at understanding rotational and clustering effects in light nuclear systems. Further experimental and theoretical efforts are essential for definitive spin-parity assignments and a complete understanding of the underlying nuclear structure.

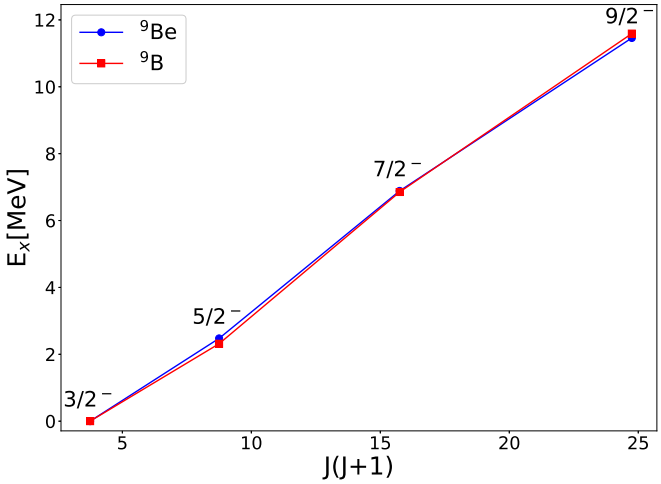

FIG. 12: Rotational band of the ground state proposed here, with highest measured states as $9/2^{-}$ members.

SUMMARY

In this work, the symmetric ^{10}B+^{10}B reaction was employed as a powerful tool to simultaneously investigate mirror nuclei in the mass region $A = 9$–11. This approach enabled a systematic study of isospin-dependent structural effects across the ^{9}Be–^{9}B, ^{10}Be–^{10}C, and ^{11}B–^{11}C mirror pairs under identical reaction conditions. The observed excitation spectra reveal clear signatures of mirror symmetry, while the measured excitation energy differences serve as sensitive indicators of underlying nuclear structure.

A distinct separation is observed between compact, shell-model-like states—characterized by small excitation energy shifts—and spatially extended cluster states, where larger deviations are consistent with Thomas–Ehrman like behavior. Several longstanding experimental questions have been addressed, including the identification of a new resonance in ^{10}C, the observation of high-spin states in the ^{11}B–^{11}C pair, and the confirmation of a high degree of symmetry in the excitation patterns of the ^{9}Be–^{9}B system.

This experiment represents the first in a broader program aimed at using symmetric light-ion reactions to probe mirror symmetry and cluster phenomena in light nuclei. The results presented here demonstrates the effectiveness of such reactions in accessing a wide range of nuclear excitations with high selectivity and resolution.

Overall, the results provide new constraints for theoretical models describing the coexistence of shell-model and cluster structures in light nuclear systems, and offer valuable benchmarks for understanding the interplay between isospin symmetry, Coulomb effects, and nuclear geometry.

ACKNOWLEDGMENTS

The authors are grateful to the LNS staff for the good-quality beam, targets and detectors.

* desa.jelavic@irb.hr

† matko.milin@phy.hr

[1] W. M. Fairbairn, Nucl. Phys. **45**, 437 (1963).
[2] K. Okamoto, Phys. Lett. **11**, 150 (1964).
[3] D.H. Wilkinson, W.D. Hay, Phys. Lett. **21**, 1, 80 (1966).
[4] J.A. Nolen Jr. and J.P. Schiffer, Annu. Rev. Nucl. Sci. **19**, 471 (1969).
[5] G. A. Miller, B. M. K. Nefkens and I. Šlaus, Phys. Rep. 194, 1 (1990).
[6] J.B. Ehrman, Phys. Rev. **81**, 3, 412 (1951).
[7] R.G.Thomas, Phys. Rev. **88**, 5, 1109 (1952).
[8] F. Everling, Nucl. Phys. A **144**, 539 (1970).
[9] S. Aoyama, K. Katō , K. Ikeda, Phys. Lett. B **414**, 13 (1997).
[10] K. Okamoto, Prog. Theor. Phys. **34**, 326 (1965).
[11] L. V. Grigorenko, T. A. Golubkova, M. V. Zhukov, Phys. Rev. C **91**, 2, 024325 (2015).
[12] M. Nakao, H. Umehara, S. Ebata and M. Ito, Phys. Rev. C **98**, 054318 (2018).
[13] T. Baba, M. Kimura, Phys. Rev. C **99** 021303 (2019).
[14] A. D. Duisenbay *et al.*, Nucl. Phys. A **996**, 2, 121692 (2020).
[15] M. Ito, EPJ Web of Conf. **117**, 06014 (2016).
[16] D. Jelavić Malenica *et al.*, Phys. Rev. C **99**, 064318 (2019).
[17] D. Jelavić Malenica *et al.*, Eur. Phys. J. A **59**, 228 (2023).
[18] N. Ikeda, K. Tagikawa, H. Horiuchi, Prog. Theor. Phys. Suppl. extra num. (1968).
[19] W. von Oertzen, M. Freer and Y. Kanada-En'yo, Phys. Rep. 432, 43 (2006).
[20] J.P. Ebran, E. Khan, T. Nikšić, D. Vretenar, How atomic nuclei cluster, Nature 487, 341 – 344 (2012).
[21] I. Lombardo, D. Dell'Aquila, Riv. Nuovo Cim. 46, 521 (2023).
[22] P. Navrátil, J. P. Vary and B. R. Barrett, Phys. Rev. C **62**, 054311 (2000).
[23] P. Navrátil and W. E. Ormand, Phys. Rev. Lett. **88**, 152502 (2002).
[24] E. Caurier, P. Navrátil, W. E. Ormand and J. P. Vary, Phys. Rev. C **66**, 024314 (2002).
[25] S. C. Pieper, K. Varga and R. B. Wiringa, Phys. Rev. C **66**, 044310 (2002).
[26] P. Navrátil and W. E. Ormand, Phys. Rev. C **68**, 034305 (2003).
[27] P. Navrátil, V. G. Gueorguiev, J. P. Vary, W. E. Ormand, A. Nogga, Phys. Rev. Lett., **99**, 042501 (2007).
[28] N. Soić *et al.*, Europhys. Lett. **34**, 7 (1996).
[29] M. Milin *et. al.*, Nucl. Phys. A **753** 263 (2005).
[30] R. J. Charity *et al.*, Phys. Rev. C **105**, 014314 (2022).
[31] E. Caurier, G. Martínez-Pinedo, F. Nowacki, A. Poves and A.P. Zuker, Rev. Mod. Phys. **77**, 427 (2005).
[32] S. Cohen and D. Kurath, Nucl. Phys. A **73**, 1 (1965).
[33] H. Nishioka, Jour. Phys. G: Nucl. Phys. **10**, 1713 (1984).
[34] Y. Kanada-En'yo, H. Morita and F. Kobayashi, Phys. Rev. C, **91**, 054323 (2015).
[35] D. Tilley, J. Kelley, J. Godwin, D. J. Millener, J. E. Purcell, C. G. Sheu and H. R. Weller, Nucl. Phys. A **745**, 155 (2004).
[36] R. de Swiniarski, F. G. Resmini, Ch. Glashausser, A. D. Bacher, Helv. Phys. Acta **59**, 227 (1976).
[37] T. K. Nayak *et al.*, Phys. Rev. Lett. **62**, 9 (1989).
[38] H. T. Fortune, Phys. Rev. C **99**, 064305 (2019).
[39] P. J. Leask *et al.*, Phys. Rev. C **63**, 034307 (2001).
[40] A. Dote, H. Horiuchi and Y. Kanada-Enyo, Phys. Rev. C **56**, 1844 (1997)
[41] N. Itagaki and S. Okabe, Phys. Rev. C 61, 044306 (2000).
[42] Y. Ogawa, K. Arai, Y. Suzuki, and K. Varga, Nucl. Phys. A 673, 122 (2000).
[43] M. J. Schneider, B. W. Ridley, M. E. Rickey, J. J. Kraushaar and W. R. Zimmerman, Phys. Rev. C **12**, 335 (1975).
[44] R. J. Charity, T. D. Wiser, K. Mercurio, R. Shane, L. G. Sobotka, A. H. Wuosmaa, A. Banu, L. Trache and R. E. Tribble, Phys. Rev. C **80**, 024306 (2009).
[45] V. Z. Goldberg and G. V. Rogachev, Phys. Rev. C **86** 044314 (2012).
[46] J. H. Kelley, E. Kwan, J. E. Purcell, C. G. Sheu and H. R. Weller, Nucl. Phys. A **880**, 88 (2012).
[47] A. N. Kuchera *et. al.*, Phys. Rev. C, **84**, 054615 (2011).
[48] S. Hamada, M. Yasue, S. Kubono, M. H. Tanaka and R. J. Peterson, Phys. Rev. C **49**, 3192 (1994).
[49] H. G. Bohlen, T. Dorsch, Tz. Kokalova, W. von Oertzen, Ch. Schulz and C. Wheldon, Phys. Rev. C **75**, 054604 (2007).
[50] M. Majer et al., Eur. Phys. J. A **43**, 153 (2010).
[51] P. H. Barker and P. A. Amundsen, Phys. Rev. C **58**, 2571 (1998).
[52] N. Soić *et al.*, Nucl. Phys. A **742**, 271 (2004).
[53] M. Freer et al. Phys. Rev C **85**, 014304 (2012).
[54] H. Yamaguchi, Phys. Rev. C **87**, 034303 (2013).
[55] L. Palada *et al.*, Acta Phys. Pol. B **17**, 3 (2024).
[56] N. Soić *et al.*, Jour. Phys. G: Nucl. Part. Phys. **31** S1701 (2005).
[57] Y. Kanada-En'yo, Phys. Rev. C **75**, 024302 (2007).
[58] J. R. Comfort, H. T. Fortune, J. V. Mahler and B. Zeidman, Phys. Rev. C, **3**, 1086 (1971).
[59] H. T. Fortune, H. G. Bingham, J. D. Garret and R. Middleton, R., Phys. Rev. C, **7**, 136 (1973).
[60] W. Bohne *et al.*, Nucl. Phys A **157**, 2, 593 (1970).
[61] G. Mutchler *et al.*, Nucl. Phys A **172**, 3, 469. (1972).
[62] D. Jelavić Malenica, Ph.D. thesis, University of Zagreb (2015).
[63] C. Adler, T. Corcoran, and C. Mast, Nucl. Phys. **88**, 145. (1966).
[64] H. G. Clerc, K. J. Wetzel and E. Spamer, Nucl. Phys. A **120**, 441 (1968).
[65] K. Arai, Y. Ogawa, Y. Suzuki and K. Varga, Phys. Rev. C, **54**, 132 (1996).
[66] M. J. Jakobson, Phys. Rev. **123**, 229 (1961).
[67] D. Rendić, N. D. Gabitzsch, V. Valković and W.V. Witsch, W.V. Nucl. Phys. A **178**, 49 (1971).
[68] S. Dixit *et al.*, Phys. Rev. C **43**, 1758 (1991).
[69] J. P. Glickman, *et. al.*, Phys. Rev. C **43**, 1740 (1991).
[70] Y. Hirayama et al., Phys. Rev. C **91**, 024328 (2015).
[71] B. Pugh, Ph.D. Thesis, MIT (1985).
[72] T. D. Baldwin *et al.*, Phys. Rev. C **86** 034330 (2012).
[73] V. Della Rocca and F. Iachello, F., Nucl. Phys. A **973**, 1, (2018).